DDMA-MIMO Observations With the MU Radar: Validation by Measuring a Beam Broadening Effect

Tomoya Matsuda and Hiroyuki Hashiguchi

***Abstract*—The phased-array radar, basically developed with the defense systems, has mainly utilized for the atmospheric radar and the wind profiling radar in the field of meteorological remote sensing, and recently it has also applied to the weather radar for research purposes. As a further development of phased-array technology, the "multiple-input–multiple-output (MIMO) technique," which has been developed in the field of communication systems, has been applied to radars. With the MIMO radar, it is possible to create a virtual antenna aperture plane beyond the actual antenna and to reduce the actual antenna size compared to that of the conventional antenna while maintaining the angular resolution. This effect is expected to reduce costs, which is one of the major hurdles in expanding phased array radars instead of parabolic antenna systems. In order to confirm the effect, an experimental observation was performed using the MU radar which is a VHF-band phased array atmospheric radar with multichannel receivers. The MIMO technique requires orthogonal waveforms on each transmitter to identify the transmitted signals with multiple receivers, and various methods are known to realize orthogonality. In this article, we focus on the "Doppler division multiple access (DDMA)" MIMO technique, with which slightly different frequencies are selected as transmit waveforms to separate in each receiver in the Doppler frequency domain. The observation results by measuring a beam broadening effect with the MU radar indicate that it will be a key technique for the atmospheric radar in the near future.**

***Index Terms*—Atmospheric radar, Doppler division multiple access, multiple-input multiple output (MIMO), phased array.**

I. Introduction

THE phased-array radar, developed by defensive radars, has been mainly utilized for the atmospheric radar and the wind profiling radar and recently, it has also been applied to the weather radar for research purposes. As a further development of the phased-array technology, "multiple-input–multiple-output (MIMO) technique," which was developed in the field of communication systems, has been applied to radars.

In recent years, various phased-array applications have been developed which performs digital beam forming (DBF) with multiple receivers. By using this technique, we can obtain multiple receive beams in a single scan, which reduces the time interval dramatically; however, in general, conventional phased array radars have no function that each transmit signal can be distinguished at the receivers, therefore, they are categorized as a "single-input–multiple-output (SIMO)" radar.

The MU radar, e.g., [1], [2], which has been operated for more than 30 years with 465 multiple transmitters, phase shifters, and corresponding antennas to orient the direction of electrically, is one of the advanced atmospheric radars and has been operated as an SIMO radar, whereas it can be also operated as an MIMO radar with additional settings explained later.

The most definitive difference between SIMO and MIMO radars is the orthogonality of the transmitter signal. A phased-array radar that separates the transmit waves can be called "multiple-input" transmitters and it is important to understand how we can separate transmit waves from the receive signals at the targets. It should be noted that adopting orthogonal waveforms in each transmitter can separate transmit waves. To realize their orthogonalities, some methods have been introduced by Sun et al. [3] in which each method has its own limitation and significance to choose the correct method for various applications.

In addition, it is necessary to consider not only the phase differences between receive signals but also those between transmit signals to create a virtual antenna aperture. For this reason, the coherent MIMO radar, which provides more capable antennas, will be discussed in this article.

The MIMO radar can be expected to improve angular resolution as described before, whereas, 3-D-high-resolution observations has been already achieved with multiple frequencies and multiple receivers. This technique is based on the combination of range imaging (RIM) toward the range direction with frequency offsets and Fourier or Capon beamformer toward spatial distribution with multiple antenna arrays [4]. The MIMO technique is similar to these methods, however, quite different from the point that it is realized by using orthogonality of transmit signals which are radiated simultaneously. This fact implies MIMO radar can be combined to the 3-D radar imaging technique which has been researched before, toward horizontal space.

An MIMO approach for the atmospheric radars has been applied by Urco et al. [5], [6] for atmospheric and ionospheric synthesis radar imaging observation, trying to use "time division multiple access (TDMA)," "code division multiple access (CDMA)" and a polarization diversity method. In this article, the DDMA method, which is useful for lower frequency radar and is superior to TDMA in terms of information density [7], is adopted and the first observation result is introduced after discussing the signal model of the MIMO radar and the revised system of the

Manuscript received 15 April 2022; revised 2 July 2022, 24 September 2022, 10 January 2023, and 4 February 2023; accepted 11 March 2023. Date of publication 16 March 2023; date of current version 31 March 2023. This work was partially supported by ISHIZUE 2022 of Kyoto University. *(Corresponding author: Tomoya Matsuda.)*

The authors are with the Research Institute for Sustainable Humanosphere, Kyoto University, Uji 611-0011, Japan (e-mail: matsuda.tomoya.22w@st.kyoto-u.ac.jp; hasiguti@rish.kyoto-u.ac.jp).

Digital Object Identifier 10.1109/JSTARS.2023.3258139

MU radar. However, it causes gain loss, because of the transmit resources are used for increment of capable receive antennas. The gain depends on the MIMO array layout and evaluated by Liao et al. [8].

The basic principle, which covers the effect of target Doppler velocities, amplitude, and phase differences between transmitters, is reviewed in Section II. The theory of the DDMA-MIMO signal model, which utilizes slow-time domain, is presented in Section III. The system configuration of the MU radar as a MIMO radar, observation results, and the future work are described in Section IV. Finally, the effectiveness of the MIMO radar is summarized in Section V.

II. MIMO Radar

A. Basic Principle

Let the M transmit signals, mth transmit signal be $x_m(t,\theta_0) = a_m(\theta_0)\phi_m(t)$ and the nth receive signal $y_n(t,\theta_0)$ is defined as

$$\begin{aligned} y_n(t,\theta_0) &= \alpha b_n(\theta_0)\sum_{m=1}^{M} a_m(\theta_0)\phi_m(t) + v_n(t) \\ &= \alpha b_n(\theta_0)\mathbf{a}(\theta_0)^{\mathrm{T}}\boldsymbol{\phi}(t) + v_n(t) \end{aligned} \tag{1}$$

where $v_n(t)$ is receive noise, $a_m(\theta_0)$ and $b_n(\theta_0)$ are transmit and receive phase shifts corresponding to the target angle θ_0, $\boldsymbol{\phi}(t) \in \mathbb{C}^M$ is a normalized transmit waveform column vector composed of M transmitters, $\mathbf{a}(\theta_0) \in \mathbb{C}^M$ is a transmit steering column vector corresponding to the transmission angle θ_0, and α is a (complex-valued) backscatter coefficient.

To expand $y_n(t,\theta_0)$ to the N receivers, a receive signal column vector $\mathbf{y}(t,\theta_0) \in \mathbb{C}^N$ is defined as

$$\mathbf{y}(t,\theta_0) = \alpha\mathbf{b}(\theta_0)\mathbf{a}(\theta_0)^{\mathrm{T}}\boldsymbol{\phi}(t) + \mathbf{v}(t) \tag{2}$$

where $\mathbf{b}(\theta_0) \in \mathbb{C}^N$ is a receive steering column vector corresponding to receive angle θ_0 (in this case, transmit and receive angles are defined to be the same), and $\mathbf{v}(t) \in \mathbb{C}^N$ is a receive noise-column vector. Note that $\mathbf{b}(\theta_0)\mathbf{a}(\theta_0)^{\mathrm{T}}$ becomes $N \times M$ matrix, that is, $\mathbf{b}(\theta_0)\mathbf{a}(\theta_0)^{\mathrm{T}} \in \mathbb{C}^{(N,M)}$.

After range processing with time lag τ and matched filters $\boldsymbol{\phi}(t-\tau)^{\mathrm{H}}$ (suffix H means Hermitian transpose) to separate the transmit waveforms, the receive signal matrix $\mathsf{Z}(\theta_0) \in \mathbb{C}^{(N,M)}$ is written as ([9], [10])

$$\begin{aligned} \mathsf{Z}(\theta_0,\tau) &\equiv \int_{-\infty}^{\infty} \mathbf{y}(t,\theta_0)\boldsymbol{\phi}(t-\tau)^{\mathrm{H}}\mathrm{d}t \\ &= \alpha\mathbf{b}(\theta_0)\mathbf{a}(\theta_0)^{\mathrm{T}}\int_{-\infty}^{\infty}\boldsymbol{\phi}(t)\boldsymbol{\phi}(t-\tau)^{\mathrm{H}}\mathrm{d}t \\ &\quad + \int_{-\infty}^{\infty}\mathbf{v}(t)\boldsymbol{\phi}(t-\tau)^{\mathrm{H}}\mathrm{d}t \\ &= \alpha\mathbf{b}(\theta_0)\mathbf{a}(\theta_0)^{\mathrm{T}}\mathsf{R}_{\boldsymbol{\phi}}(\tau) + \mathsf{E}(\tau) \end{aligned} \tag{3}$$

where

$$\mathsf{R}_{\boldsymbol{\phi}}(\tau) \equiv \int_{-\infty}^{\infty}\boldsymbol{\phi}(t)\boldsymbol{\phi}(t-\tau)^{\mathrm{H}}\mathrm{d}t \quad \in \mathbb{C}^{(M,M)} \tag{4}$$

is the $M \times M$ MIMO signal correlation matrix that describes the correlation among the transmit waveforms, and

$$\mathsf{E}(\tau) \equiv \int_{-\infty}^{\infty}\mathbf{v}(t)\boldsymbol{\phi}(t-\tau)^{\mathrm{H}}\mathrm{d}t \quad \in \mathbb{C}^{(N,M)} \tag{5}$$

is the filtered receive noise matrix.

The $N \times M$ data matrix of (3) may be vectorized by stacking its columns of $\mathsf{Z}(\theta_0,\tau)$ and we define the receive MIMO signal by

$$\mathbf{z}(\theta_0,\tau) \equiv \mathrm{vec}[\mathsf{Z}(\theta_0,\tau)] \quad \in \mathbb{C}^{(NM,1)}. \tag{6}$$

Equation (6) is rewritten with the well-known relationships of the vectorization operator shown as [11]

$$\begin{aligned} \mathrm{vec}\{\mathsf{XYZ}\} &= \{\mathsf{Z}^{\mathrm{T}} \otimes \mathsf{X}\}\mathrm{vec}\{\mathsf{Y}\} \\ \mathrm{vec}\{\mathsf{XYZ}\} &= \{\mathsf{Z}^{\mathrm{T}} \otimes \mathsf{I}_N\}\mathrm{vec}\{\mathsf{XY}\} \\ \mathrm{vec}\{\mathsf{XY}^{\mathrm{T}}\} &= \{\mathsf{Y} \otimes \mathsf{X}\} \end{aligned} \tag{7}$$

where X is an arbitrary $N \times K$ matrix, Y is an arbitrary $K \times L$ matrix, Z is an arbitrary $L \times N$ matrix, I_N is a unit matrix of $N \times N$, and "$\otimes$" indicates the Kroneker product

$$\begin{aligned} \mathbf{z}(\theta_0,\tau) &= \mathrm{vec}[\alpha\mathbf{b}(\theta_0)\mathbf{a}(\theta_0)^{\mathrm{T}}\mathsf{R}_{\boldsymbol{\phi}}(\tau)] + \mathrm{vec}[\mathsf{E}(\tau)] \\ &= \alpha[\mathsf{R}_{\boldsymbol{\phi}}^{\mathrm{T}}(\tau) \otimes \mathsf{I}_N]\mathrm{vec}[\mathbf{b}(\theta_0)\mathbf{a}(\theta_0)^{\mathrm{T}}] + \mathrm{vec}[\mathsf{E}(\tau)] \\ &= \alpha[\mathsf{R}_{\boldsymbol{\phi}}^{\mathrm{T}}(\tau) \otimes \mathsf{I}_N][\mathbf{a}(\theta_0) \otimes \mathbf{b}(\theta_0)] + \mathrm{vec}[\mathsf{E}(\tau)] \\ &\equiv \alpha\mathbf{s}(\theta_0,\tau) + \mathbf{e}(\tau) \end{aligned} \tag{8}$$

where the MIMO steering vector $\mathbf{s}(\theta_0,\tau)$ for the beam angle θ_0 and the filtered noise columns vector $\mathbf{e}(\tau)$ are defined as

$$\mathbf{s}(\theta_0,\tau) \equiv [\mathsf{R}_{\boldsymbol{\phi}}^{\mathrm{T}}(\tau) \otimes \mathsf{I}_N][\mathbf{a}(\theta_0) \otimes \mathbf{b}(\theta_0)] \tag{9}$$

$$\mathbf{e}(\tau) \equiv \mathrm{vec}[\mathsf{E}(\tau)]. \tag{10}$$

If we assume that the transmit signals of $\boldsymbol{\phi}(t)$ are orthogonal with each other and that each matched filtered range response is identical defined as $R_{\boldsymbol{\phi}}(\tau)$, then each element of MIMO signal correlation matrix can be expressed as

$$\begin{aligned} \{\mathsf{R}_{\boldsymbol{\phi}}(\tau)\}_{mm'} &\equiv \int_{-\infty}^{\infty}\phi_m(t)\phi_{m'}^{*}(t-\tau)\mathrm{d}t \\ &= \begin{cases} R_{\boldsymbol{\phi}}(\tau), & (\text{for } m = m') \\ 0, & (\text{for } m \neq m') \end{cases} \end{aligned} \tag{11}$$

and (8) is rewritten as

$$\mathbf{z}(\theta_0,\tau) = \alpha R_{\boldsymbol{\phi}}(\tau)[\mathbf{a}(\theta_0) \otimes \mathbf{b}(\theta_0)] + \mathbf{e}(\tau). \tag{12}$$

According to (12), the radar can utilize its transmit freedom called the MIMO steering matrix, which is expressed as $\mathbf{a}(\theta_0) \otimes \mathbf{b}(\theta_0) \in \mathbb{C}^{(NM,1)}$, by transmitting orthogonal waveforms. Fig. 1 shows the principal image of the MIMO radar with transmit orthogonality in the case of $M = N = 3$.

B. Principle With Doppler Effect, Transmit Amplitude, and Phase Difference

The ideal transmit signals are expressed as $\mathbf{x}(t,\theta_0) = \mathbf{a}(\theta_0) \odot \boldsymbol{\phi}(t)$ using the Hadamard product $\odot$. However, in an

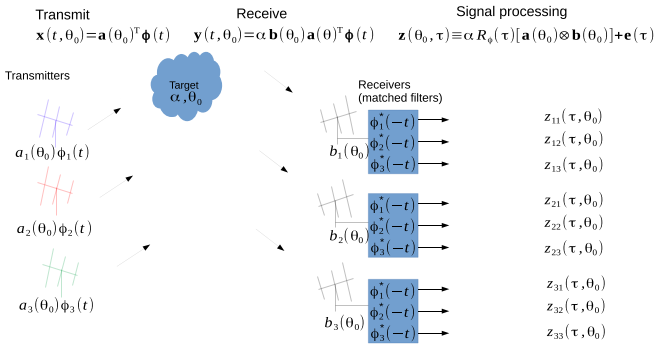

Fig. 1. Principle image of the MIMO radar. Transmit signals are divided by matched filters in each receiver.

actual radar system, we must consider where and how we execute the matched filter process.

In general, the matched filter $\boldsymbol{\phi}(t)^{\mathrm{H}}$ is not applied directly because the transmit power is too high to measure the waveforms. To overcome this limitation, a low-power signal was used as the reference signal.

We may decide to redefine the reference signal as the point before high-power amplifiers, and the transmit waveform is replaced as

$$\boldsymbol{\phi}(t) \Rightarrow \mathbf{p} \odot \boldsymbol{\phi}(t) \tag{13}$$

where $\mathbf{p} \in \mathbb{C}^M$ is the (time constant) amplitude and phase offset function usually caused by hardware difference between transmitters.

The transmitter amplitude and phase offset function $\mathbf{p}$ can be expressed as

$$\mathbf{p} = [A_1 \mathrm{e}^{-\mathrm{j}\delta_1}, \cdots, A_m \mathrm{e}^{-\mathrm{j}\delta_m}, \ldots, A_M \mathrm{e}^{-\mathrm{j}\delta_M}]^{\mathrm{T}} \tag{14}$$

where A_m is the amplitude offset and δ_m is the phase offset in the mth transmitter.

Equation (2) is rewritten by considering the Doppler shift from the target as follows:

$$\mathbf{y}(t,\theta_0) = \alpha \mathrm{e}^{\mathrm{j}2\pi\nu t}\mathbf{b}(\theta_0)\mathbf{a}(\theta_0)^{\mathrm{T}}[\mathbf{p}\odot\boldsymbol{\phi}(t)] + \mathbf{v}(t) \tag{15}$$

where $\alpha \mathrm{e}^{\mathrm{j}2\pi\nu t}$ is the complex backscatter coefficient with Doppler shift frequency of the target ν.

Equation (3) added by Doppler term is also written as

$$\begin{aligned}\mathsf{Z}(\theta_0,\tau,\nu) &= \alpha\mathbf{b}(\theta_0)\mathbf{a}(\theta_0)^{\mathrm{T}}\int_{-\infty}^{\infty}[\mathbf{p}\odot\boldsymbol{\phi}(t)]\boldsymbol{\phi}(t-\tau)^{\mathrm{H}}\mathrm{e}^{\mathrm{j}2\pi\nu t}\mathrm{d}t \\ &\quad + \int_{-\infty}^{\infty}\mathbf{v}(t)\boldsymbol{\phi}(t-\tau)^{\mathrm{H}}\mathrm{d}t \\ &\equiv \alpha\mathbf{b}(\theta_0)\mathbf{a}(\theta_0)^{\mathrm{T}}\mathrm{diag}(\mathbf{p})\mathsf{X}_{\boldsymbol{\phi}}(\tau,\nu) + \mathsf{E}(\tau)\end{aligned} \tag{16}$$

where $\mathrm{diag}(\mathbf{p})$ denotes the diagonal matrix of vector $\mathbf{p}$, and $\mathsf{X}_{\boldsymbol{\phi}}(\tau,\nu)$ is the ambiguity function matrix [12] defined as

$$\mathsf{X}_{\boldsymbol{\phi}}(\tau,\nu) \equiv \int_{-\infty}^{\infty}\boldsymbol{\phi}(t)\boldsymbol{\phi}(t-\tau)^{\mathrm{H}}\mathrm{e}^{\mathrm{j}2\pi\nu t}\mathrm{d}t. \tag{17}$$

The exponential term of (17) implies that the off-diagonal components of the correlation matrix does not always become zero, and therefore cannot maintain orthogonality between the transmitters due to the target Doppler shift.

However, when dealing with pulsed Doppler radars having a pulse repetition time T_{IPP}, the integration time is within the pulsewidth time t_w, and the target velocities are relatively small, the Doppler term can be taken as a constant value around $t = \tau$. For example, if ν and t_w are taken to keep $|2\pi\nu t_w| < 0.01$ radian (0.57°) phase rotation in the pulse length, the exponential term can be taken as the same value while pulsewidth duration.

This is good approximation because it considers the exponential term as a constant during integration to divide this term into the correlation part and the following equations are derived [13]:

$$\mathsf{X}_{\boldsymbol{\phi}}(\tau,\nu) \approx \int_0^{T_{IPP}}\boldsymbol{\phi}(t)\boldsymbol{\phi}(t-\tau)^{\mathrm{H}}\mathrm{d}t \equiv \mathsf{R}_{\boldsymbol{\phi}}(\tau) \tag{18}$$

where τ denotes the correlation time of T_{IPP} duration.

Clearly, from (18), we can separate the target Doppler component from the MIMO signal correlation matrix. This separation makes the radar hardware configuration easier, which means that the fast time signal processing (corresponding to the integration time) and the slow time signal processing (corresponding to the discrete time) can be independently constructed. Note that the term of $\mathrm{e}^{\mathrm{j}2\pi\nu\tau}$, phase rotation by time lag, is multiplied by all the components commonly, therefore it will be omitted to simplify the equations.

The products of the target Doppler velocities and the pulse length should also be considered to keep the value small. Table I shows an example of phase rotation in the fast-time signal processing substituted by the typical transmit frequency, pulse length, and maximum Doppler velocity of the target. From this table, it can be seen that the Doppler effect is negligible for the lower frequency radar; however, it may influence the assumption when using *L*-band or *C*-band radio frequency.

As described before, two conditions of lower transmit frequency and small target Doppler speed are enabled to establish the approximation in (18), which Doppler ambiguity term has been deleted. The MU radar, radiates VHF transmit frequency (46.5 MHz) and normally $< 20\,\mathrm{ms}^{-1}$ target, may have the decision to apply this approximation; however, there would be a case that Doppler ambiguity cannot be ignored, (17) needs be strictly applied with the consideration of Doppler ambiguity. In general, the choice of DDMA is recommended for lower transmit frequency.

TABLE I
EXAMPLE OF DOPPLER TERM INFLUENCE ON THE PHASE ROTATION WITHIN THE TRANSMIT PULSE SEQUENCE ($\nu = 2(F/\mathrm{C})v_{td}$)

No.	Transmit freq. f (MHz)	Pulse width t_w (μs)	Doppler speed Max.v_d (ms^{-1})	Doppler freq. Max.ν (Hz)	Phase rotation $2\pi\nu t_w$ (rad)
1	50	50	90.0	30.0	0.009
2	1000	50	20.0	133.3	0.042
3	5000	50	10.0	333.3	0.105

III. DDMA-MIMO Observation

DDMA-MIMO method is commonly used and has proved the effectiveness of its orthogonality (e.g., [14], [15]), whereas Sun et al. [3] has pointed out that it requires wide Doppler unambiguity so that lower frequency radar is suitable in general.

In this section, L pulse trains transmit waveforms are introduced to discuss more specifically to discuss DDMA-MIMO principle, which leads to clarify the important points when applying DDMA-MIMO method to the MU radar.

A. Expansion to L Pulse Trains

Let lth transmit pulse train waveforms $\{\mathbf{u}(t)\}_l \in \mathbb{C}^M$ (l takes 0 to $L-1$ for slow-time direction), lth ambiguity function matrix $\{\mathsf{X}_{\boldsymbol{\phi}}(\tau,\nu)\}_l \in \mathbb{C}^{(M,M)}$, summation of ambiguity function $\mathsf{X}_{\boldsymbol{\phi}}(\tau,\nu) \in \mathbb{C}^{(M,M)}$, lth filtered receive noise matrix $\{\mathsf{E}(\tau)\}_l \in \mathbb{C}^{(N,M)}$, lth filtered noise columns vector $\{\mathbf{e}(\tau)\}_l \in \mathbb{C}^{(MN,1)}$, and summation of noise columns vector $\mathbf{e}(\tau) \in \mathbb{C}^{(MN,1)}$ using the lth receive noise column vector $\{\mathbf{v}(t)\}_l \in \mathbb{C}^N$ as [16]

$$\{\mathbf{u}(t)\}_l \equiv \boldsymbol{\phi}(t - lT_{IPP}) \tag{19}$$

$$\{\mathsf{X}_{\boldsymbol{\phi}}(\tau,\nu)\}_l \equiv \int_0^{T_{IPP}} \{\mathbf{u}(t)\}_l \{\mathbf{u}(t-\tau)\}_l^{\mathrm{H}} \mathrm{d}t \tag{20}$$

$$\mathsf{X}_{\boldsymbol{\phi}}(\tau,\nu) \equiv \sum_{l=0}^{L-1} \{\mathsf{X}_{\boldsymbol{\phi}}(\tau,\nu)\}_l \tag{21}$$

$$\{\mathsf{E}(\tau)\}_l \equiv \int_0^{T_{IPP}} \{\mathbf{v}(t)\}_l \{\mathbf{u}(t-\tau)\}_l^{\mathrm{H}} \mathrm{d}t \tag{22}$$

$$\{\mathbf{e}(\tau)\}_l \equiv \mathrm{vec}[\{\mathsf{E}(\tau)\}_l] \tag{23}$$

$$\mathbf{e}(\tau) \equiv \sum_{l=0}^{L-1} \{\mathbf{e}(\tau)\}_l. \tag{24}$$

The ambiguity function of periodic pulse radar signals $\mathsf{X}(\tau,\nu)$ can be expressed by [13]

$$\mathsf{X}(\tau,\nu) \approx \mathsf{R}_{\boldsymbol{\phi}}(\tau) \sum_{l=0}^{L-1} \mathrm{e}^{\mathrm{j}2\pi\nu l T_{IPP}} \tag{25}$$

on condition that product of the target Doppler shift frequency times pulsewidth $\nu t_w \approx 0$ and the influence of second trip echoes is not affected in the signal processing described before. The receive MIMO signal added to the target Doppler shift is rewritten from (16)

$$\begin{aligned}\mathbf{z}(\theta_0,\tau,\nu) &\equiv \alpha\left\{\mathrm{diag}(\mathbf{p})\mathsf{X}_{\boldsymbol{\phi}}^{\mathrm{T}}(\tau,\nu) \otimes \mathsf{I}_N\right\} \cdot [\mathbf{a}(\theta_0) \otimes \mathbf{b}(\theta_0)] + \mathbf{e}(\tau) \\ &\equiv \alpha \mathrm{diag}(\mathbf{p})\mathbf{s}[\theta_0,\tau,\nu] + \mathbf{e}(\tau)\end{aligned} \tag{26}$$

where the MIMO steering vector for the beam angle θ_0, lag time τ and the target Doppler frequency ν is defined as

$$\mathbf{s}(\theta_0,\tau,\nu) \equiv \left\{\mathsf{X}_{\boldsymbol{\phi}}^{\mathrm{T}}(\tau,\nu) \otimes \mathsf{I}_N\right\} \cdot [\mathbf{a}(\theta_0) \otimes \mathbf{b}(\theta_0)] \tag{27}$$

and lth pulse train component $\mathbf{s}(\theta_0,\tau,\nu,l)$ is also expressed as

$$\mathbf{s}(\theta_0,\tau,\nu,l) \equiv \left(\{\mathsf{X}_{\boldsymbol{\phi}}^{\mathrm{T}}(\tau,\nu)\}_l \otimes \mathsf{I}_N\right) \cdot [\mathbf{a}(\theta_0) \otimes \mathbf{b}(\theta_0)]. \tag{28}$$

B. DDMA-MIMO Principle

The DDMA method utilizes the pulse-to-pulse phase difference, which is derived from the Doppler effect, and slightly different frequencies are selected as transmit waveforms to be separated in the Doppler frequency domain.

The DDMA can divide their transmit signals with Doppler division, which means that we can use time slots per interpulse period (or pulse-repetition-frequency), called the "slow-time" direction. Therefore, DDMA is executed after the ranging process [17]. In other words, the range response process and orthogonal transmit signal separation process are divided when using the slow-time direction.

DDMA requires a transmit phase difference of $2\pi f_{md}$ between T_{IPP} to obtain the orthogonality of the transmitter, and transmit signals $\mathbf{u}(t) \in \mathbb{C}^{(M,L)}$ is defined as [16]

$$\{\mathbf{u}(t)\}_l \equiv [\mathbf{w}_l(t) \odot \mathbf{f}_l(t)] \cdot \phi(t - lT_{IPP}) \tag{29}$$

$$\{\mathbf{w}(t)\}_{m,l} = [\mathrm{e}^{\mathrm{j}\{\mathbf{p}(t)\}_{1,l}}, \ldots, \mathrm{e}^{\mathrm{j}\{\mathbf{p}(t)\}_{m,l}}, \ldots, \mathrm{e}^{\mathrm{j}\{\mathbf{p}(t)\}_{M,l}}]^{\mathrm{T}} \tag{30}$$

$$\{\mathbf{f}(t)\}_{m,l} = 1 \tag{31}$$

$$\begin{aligned}\{\mathbf{p}(t)\}_{m,l} &\equiv 2\pi(m-1)f_{md}\left\lfloor \frac{t}{T_{IPP}} \right\rfloor T_{IPP} \\ &= 2\pi(m-1)f_{md} l T_{IPP}[-3pt]\end{aligned} \tag{32}$$

where $\mathbf{w}(t) \in \mathbb{C}^{(M,L)}$ and $\mathbf{f}(t) \in \mathbb{C}^{(M,L)}$ are the column vectors of the phase and frequency offset of the transmitters, $\mathbf{w}_l(t) \in \mathbb{C}^M$ and $\mathbf{f}_l(t) \in \mathbb{C}^M$ are the column components of $\mathbf{w}(t)$ and $\mathbf{f}(t)$, $\{\mathbf{p}(t)\}_{m,l}$ is the phase offset at mth transmitter and lth pulse train, $\lfloor\ \rfloor$ indicates the floor function, respectively.

The (m,m') element of the DDMA-MIMO ambiguity function matrix of the lth pulse train is expressed as

$$\begin{aligned}&\{\mathsf{X}(\tau,\nu)\}_{mm,'l} \\ &= \mathrm{e}^{\mathrm{j}2\pi\nu l T_{IPP}} \int_0^{T_{IPP}} \{\mathbf{u}(t)\}_{m,l} \cdot \{\mathbf{u}^*(t-\tau)\}_{m,'l} \mathrm{d}t \\ &= \mathrm{e}^{\mathrm{j}2\pi\nu l T_{IPP}} \int_0^{T_{IPP}} [\mathrm{e}^{\mathrm{j}\{\mathbf{p}(t)\}_{m,l}} \phi(t)][\mathrm{e}^{\mathrm{j}\{\mathbf{p}^*(t-\tau)\}_{m,'l}} \phi^*(t-\tau)] \mathrm{d}t \\ &= \mathrm{e}^{\mathrm{j}2\pi\nu l T_{IPP}} \int_0^{T_{IPP}} [\phi(t)\phi^*(t-\tau)] \left[\mathrm{e}^{\mathrm{j}2\pi(m-m')f_{md} l T_{IPP}}\right] \mathrm{d}t \\ &= R_\phi(\tau) \cdot \mathrm{e}^{\mathrm{j}2\pi\nu l T_{IPP}} \cdot \mathrm{e}^{\mathrm{j}2\pi[(m-m')f_{md}] l T_{IPP}}.\end{aligned} \tag{33}$$

Now we focus on the second exponential component of (33). In general, the discrete Fourier transformation toward $t_l = lT_{IPP}(l = 0, 1, 2 \cdots L-1)$ (time series of every T_{IPP}) is executed instead of the summation according (21), and the frequency distribution toward $f_l = 1/(lT_{IPP})$ is defined by the expression with Fourier transform expression "$\mathcal{F}$" as follows:

$$\begin{aligned}&\{\mathsf{X}_{\boldsymbol{\phi}}(\tau,\nu)\}_{mm,'f_l} \\ &\equiv \mathcal{F}\left(\{\mathsf{X}_{\boldsymbol{\phi}}(\tau,\nu)\}_{mm,'t_l}\right) \\ &= R_\phi(\tau) \sum_{l=0}^{L-1} \mathrm{e}^{\mathrm{j}2\pi\nu t_l} \mathrm{e}^{\mathrm{j}2\pi[(m-m')f_{md}]t_l} \mathrm{e}^{-\mathrm{j}2\pi \cdot \frac{f_l t_l}{L}} \\ &= R_\phi(\tau) F_\nu[f_l - (m-m')f_{md}]\end{aligned} \tag{34}$$

where

$$F_\nu[f_l] \equiv \mathcal{F}[\mathrm{e}^{\mathrm{j}2\pi\nu t_l}] \tag{35}$$

is the Doppler frequency distribution of the target which depends on its characteristics.

Now, we can assume that atmospheric and/or precipitation motions which are our interests in meteorology have limited frequency distribution between minimum Doppler frequency f_{td-min} and maximum one f_{td-max}. To divide the transmitted waveforms in the receiver, DDMA uses a Doppler frequency bandpass (rectangular) filter toward the slow-time direction as

$$H[f_l] = \begin{cases} 1, & (\text{for } |f_l| < \frac{f_{md}}{2}) \\ 0, & (\text{others}) \end{cases} \tag{36}$$

and the ambiguity function multiplied Doppler frequency bandpass filter becomes

$$\begin{aligned} &\{\mathbf{X}_{\boldsymbol{\phi}}(\tau,\nu)\}_{mm,'f_l} \cdot H[f_l] \\ &= R_\phi(\tau)\left\{F_\nu[f_l-(m-m')f_{md}]\cdot H[f_l]\right\} \\ &= \begin{cases} R_\phi(\tau)F_\nu[f_l], & (\text{for } m=m') \\ 0, & (\text{others}) \end{cases} \end{aligned} \tag{37}$$

where f_{md} should be selected to keep the condition that $-f_{md}/2 < f_{td-min}$ and $f_{td-max} < f_{md}/2$.

Again, the DDMA-MIMO steering vector of lth pulse train for beam angle θ_0 and the target Doppler frequency ν after filtering process is defined as

$$\begin{aligned} \mathbf{s}[\theta_0,\tau,\nu,l] &\equiv R_\phi(\tau)\,\mathcal{F}^{-1}\left\{F_\nu[f_l]\cdot H[f_l]\right\}\cdot \\ &\quad [\mathrm{diag}(\mathbf{p})\otimes \mathbf{I}_N][\mathbf{a}(\theta_0)\otimes\mathbf{b}(\theta_0)] \\ &= R_\phi(\tau)\left\{\mathrm{e}^{\mathrm{j}2\pi\nu l T_{IPP}} * h[lT_{IPP}]\right\}\cdot \\ &\quad [\mathrm{diag}(\mathbf{p})\otimes \mathbf{I}_N][\mathbf{a}(\theta_0)\otimes\mathbf{b}(\theta_0)] \end{aligned} \tag{38}$$

where $h[lT_{IPP}] \equiv \mathrm{sinc}[f_{md}lT_{IPP}]$ is the time-domain expression of the bandpass filter and "$*$" denotes convolution integration.

Equation (38) indicates that the transmitters with DDMA have a complete orthogonality with each other if the target Doppler distribution is within the Doppler frequency bandpass filter. Although the influence of the Doppler filter has been shown to be a sinc function in (38), this effect may be minimized to apply other window functions instead of a rectangular window.

On the other hand, these ideal characteristics may require very wide Doppler unambiguity range, which restricts the maximum target range. This may cause limitations in using the radar for higher transmit frequencies.

C. DDMA-MIMO With Frequency Offset Principle

DDMA-MIMO is also realized with a transmit frequency offset slightly. We focus on the frequency offset f_{md} instead of the phase offset between transmitters the phase and frequency offset $\{\mathbf{w}(t)\}_{m,l}$ and $\{\mathbf{f}(t)\}_{m,l}$ are expressed as [16]

$$\{\mathbf{w}(t)\}_{m,l} = 1 \tag{39}$$

$$\{\mathbf{f}(t)\}_{m,l} = \left[\mathrm{e}^{\mathrm{j}\{\mathbf{p}(t)\}_{1,l}},\ldots,\mathrm{e}^{\mathrm{j}\{\mathbf{p}(t)\}_{m,l}},\ldots,\mathrm{e}^{\mathrm{j}\{\mathbf{p}(t)\}_{M,l}}\right]^{\mathrm{T}} \tag{40}$$

$$\{\mathbf{p}(t)\}_{m,l} \equiv 2\pi(m-1)f_{md}t. \tag{41}$$

Equation (41) can be written as follows [15]:

$$\begin{aligned} \{\mathbf{p}(t)\}_{m,l} &= 2\pi(m-1)f_{md}\left(\frac{t}{T_{IPP}}\right)T_{IPP} \\ &= 2\pi(m-1)f_{md}\left\lfloor\frac{t}{T_{IPP}}\right\rfloor T_{IPP} \\ &\quad + 2\pi(m-1)f_{md}(t-lT_{IPP}). \end{aligned} \tag{42}$$

The first term of the right-hand side stepped by T_{IPP} in (42) is the same as (32) and the second term means transmit signals have linear phase increment of $2\pi(m-1)f_{md}t$ toward fast-time but reset to zero by T_{IPP}. Moreover, in case that $2\pi(m-1)f_{md}t_w$ (m takes 1 to M) is relatively small, the same discussion in Section II-B can be applied that the exponential term $\exp[\mathrm{j}2\pi(m-1)f_{md}(t-lT_{IPP})]$ is regarded as the constant value at τ while integral duration toward the first time in each transmit signal.

However, this term has a unique value for the transmit position so that phase difference between transmitters need to be calibrated whereas target Doppler phase rotation is able to omitted. This range-direction phase offset defined $\mathbf{q}(\tau) \in \mathbb{C}^M$ is expressed as

$$\mathbf{q}(\tau) = \left[\mathrm{e}^{-\mathrm{j}2\pi 0 f_{md}\tau},\cdots,\mathrm{e}^{-\mathrm{j}2\pi(m-1)f_{md}\tau},\cdots,\mathrm{e}^{-\mathrm{j}2\pi(M-1)f_{md}\tau}\right]^{\mathrm{T}} \tag{43}$$

and DDMA-MIMO steering vector when using frequency offset is expressed by multiplying (43) into (38)

$$\begin{aligned} \mathbf{s}[\theta_0,\tau,\nu,l] &= R_\phi(\tau)\left\{\mathrm{e}^{\mathrm{j}2\pi\nu l T_{IPP}} * h[lT_{IPP}]\right\}\cdot \\ &\quad [\mathrm{diag}(\mathbf{p})\cdot\mathrm{diag}(\mathbf{q}(\tau))\otimes\mathbf{I}_N][\mathbf{a}(\theta_0)\otimes\mathbf{b}(\theta_0)]. \end{aligned} \tag{44}$$

For the radar system, the frequency offset method can be implemented easier than the phase offset method because the frequency accuracy is very stable and it is very easy to set up a system that only requires the addition of frequency resources for the MU radar when applying as the MIMO radar. Besides, the low frequency of the MU radar also has an advantage that the maximum offset frequency $2\pi(M-1)f_{md}w$ can be taken to almost zero to apply for DDMA.

For example, the maximum offset frequency is selected to $2(M-1)f_{md} = 30$ Hz and pulsewidth $w = 50\,\mu$s, pulse rotation becomes 0.009 rad shown as Table I that is sufficient to meet the condition. On the other hand, in the case that higher frequency for phase offset is chosen, strict evaluations with the ambiguity function may be required which has the same behavior as faster Doppler targets. In summary, the phase offset between transmitters expressed by (14) and the range-direction phase offset by (43) needs to be implemented to the signal processor from the result of (44) when constructing DDMA-MIMO radar system with frequency offset. It should be noted that DDMA

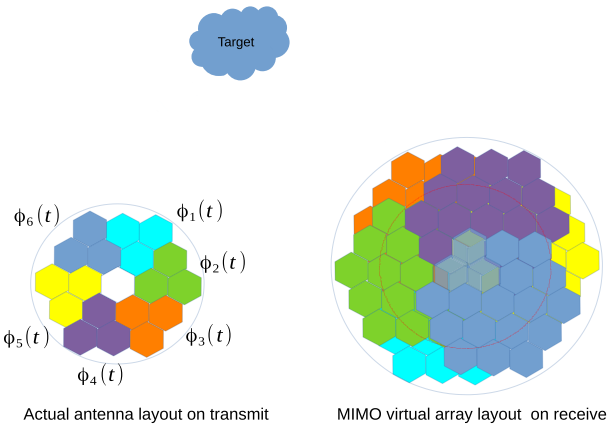

Fig. 2. Actual antenna layout on transmit (left) and MIMO virtual array layout on receive (right).

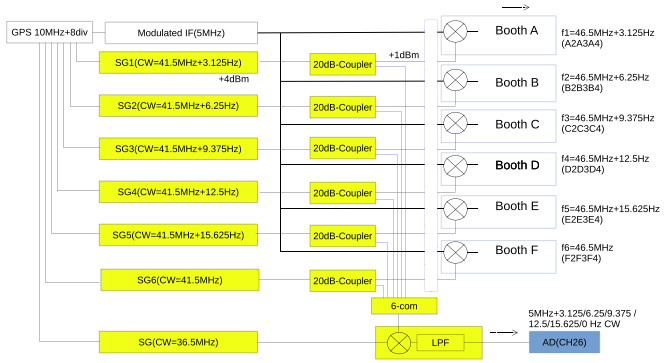

Fig. 3. DDMA-MIMO transmitter configuration with the MU radar. The yellow mark indicates additional settings, and the six orthogonal signals are distributed to the transmitters. They are also combined with the 26th synchronized receiver via couplers to detect the amplitude and phase difference between the transmitters.

with the frequency offset method uses to generate pulse-to-pulse phase difference, therefore it is not categorized as FDMA.

In general, it is known that the DDMA-MIMO channel matrix is expressed simply as $\mathbf{a}(\theta_0) \otimes \mathbf{a}_D(\nu T_{IPP}) \otimes \mathbf{b}(\theta_0)$ with the Doppler term expression $\mathbf{a}_D(\nu T_{IPP})$ shown by and [7] and [13], for example. The result of (44) is consistent to this formula if it is expressed as summation of lth pulse trains and eliminated the term of $[\mathrm{diag}(\mathbf{p}) \cdot \mathrm{diag}(\mathbf{q}(\tau)) \otimes \mathbf{l}_N]$, which means it may be used directly to the MU radar. However, the DDMA with frequency offset method and two offset corrections (amplitude/phase difference between transmitters and range phase offset on receivers) need to be explained to apply for the MU radar, therefore, this article does not use this simple formula and describes about these effects from the principles shown by [9].

IV. DDMA-MIMO Observation With the MU Radar

A. System Configuration

The MU radar [1], located in Shigaraki, Shiga, Japan, is a state-of-the-art atmospheric radar that has been under operation since 1984. It has one modulator, 475 elements of VHF-band (46.5 MHz) cross-Yagi phased array antennas, and 25 plus additional four receivers as shown in [18], therefore, it is categorized as an SIMO radar. However, this radar can also play the role of MIMO radar quite easily because of its flexibility.

Now, we can classify transmit antennas into six parts and apply orthogonal waveforms with synchronized signal generators (SGs) that have slightly different frequencies. Each receiver is divided into six orthogonal transmitter signals with Doppler matched filters to realize MIMO virtual receive array. Fig. 2 shows the actual antenna layout on transmit and the MIMO virtual array on receive image.

1) Transmitter Configuration: The transmitter configuration is shown in Fig. 3. The MU radar radiates 46.5 MHz RF transmit signal by mixing a 5 MHz modulated IF-signal and a 41.5 MHz CW-local signal, those of which are divided into six part toward to Booth A to F. Orthogonalities on transmission are realized by replacing the original local signal with a separate local signal

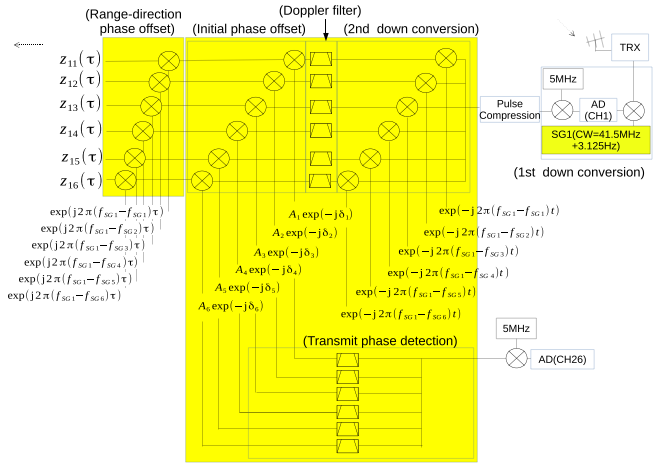

Fig. 4. DDMA-MIMO receiver configuration with the MU radar. The Doppler filter part, transmit phase detection part, transmit initial offset part, and range-direction phase offset part are shown. Yellow areas are additional setting parts of the receiver.

generated with each SG. The interesting part of this configuration is that the compensation algorithm of the amplitude and phase differences between the transmit signals, which is expressed by the diag part of (38), is added. As explained before, $\boldsymbol{\phi}(t)$ is not used as a matched filter directly, therefore, we need to know their initial amplitude and phase in the process of beam forming. To acquire amplitude and phase information of these transmit signals, 20 dB couplers are added to each transmitter to extract local signals.

2) Receiver Configuration: The receiver configuration is shown in Fig. 4. The receive echoes corresponding to each transmit signal are mixed at the signal processing stage (until the pulse compression stage). To divide into orthogonal signals, the Doppler filter toward to slow-time direction, which is described by (38), is applied. It should be noted that matched filter processes corresponding to each transmit frequency should be selected; however, the signal processing for the down conversion of the MU radar cannot be changed because the same analog

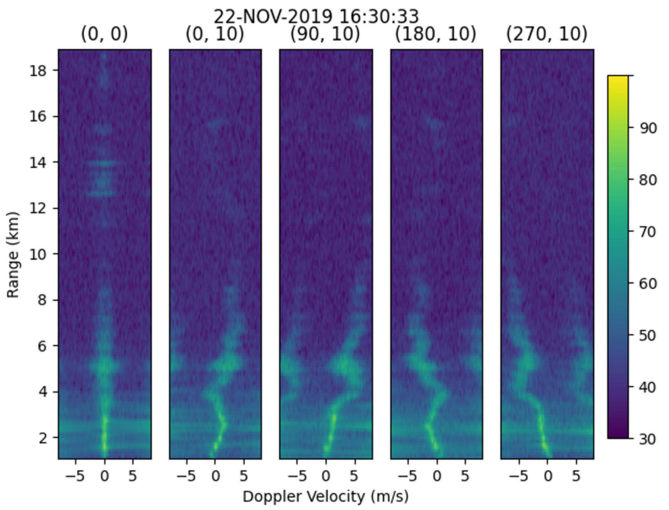

Fig. 5. DDMA-MIMO height profile observed with the MU radar at 1630 JST November 22, 2019. Horizontal axis shows target Doppler velocity, the vertical axis shows the target range (height from the ground), and warm contours indicate strong echoes. From the left picture, vertical, north-tilted, east-tilted, south-tilted, and west-tilted beam with 10° zenith angle are shown.

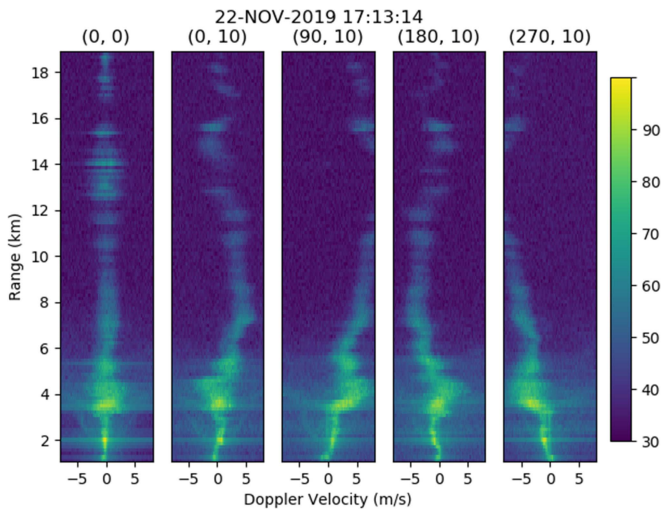

Fig. 6. Height profile observed with the MU radar (without DDMA-MIMO methods, full-scale), at 1713 JST November 22, 2019. The display method is the same as in Fig. 5.

local signals are used in each receiver and the matched filter is not adopted directly. For the above reason, we must include a digital down-conversion part to realize the DDMA-MIMO matched filter after the analog down conversion part and pulse compression part.

To digitize and synchronize the divided transmit amplitude and phase signals, an additional receiver is utilized. Their frequencies are around 41.5 MHz, so another synchronized SG (CW = 36.5 MHz) is used for the down converter to adjust the receiver's specifications (IF = 5 MHz input).

Ideally, the same number of receivers corresponding to each reference signal should be prepared; however, this could result in a shortage of receivers (in this case, six receivers are requested against four additional receivers). To overcome this limitation, we have adopted a method in which the transmit waveforms are combined in the analog region and subsequently detected by one receiver to separate them using Doppler filters during digital signal processing.

B. Observation Result

Fig. 5 shows the range-Doppler distribution observed at 1630 JST 22 Nov 2019 with the MU radar. In this case study, $f_{md} = 3.125$ Hz was selected (the Nyquist velocity is 10.08 ms^{-1}) and each transmit frequency is set to 46.500 003 125, 46.500 006 250, 46.500 009 375, 46.500 012 500, 46.500 015 625, and 46.500 018 750 MHz, respectively. From this figure, it is confirmed that the MU radar can be successfully operated as a DDMA-MIMO radar.

To compare with the original MU radar observation results, full-array observation for the MU radar was performed after executing the DDMA-MIMO observation and setting it back to the original configuration. On comparing Figs. 5 and 6, it can be seen that the full-array observation results have stronger echoes than that of the DDMA-MIMO observation; however, the result of the DDMA-MIMO has shown a narrower spectral beam width, especially around the range of 4–6 km.

It should be noted that the orthogonal transmit signal interval is set to 3.125 Hz which is corresponded to 10.078 m/s Doppler speed, therefore aliased echoes caused by adjacent transmit signal are seen in Fig. 5. The reason is that atmospheric echoes has around 2–5 m/s Doppler shift, which becomes visible appearing beyond (fixed) Doppler filters. It has a possibility to degrade the orthogonality in general, however, in this case it can keep orthogonalities, because that adjacent echoes are not overlapped with each other obviously from the Fig. 5.

It is also noted that it is important for DDMA not to become invisible adjacent transmit signals by filter, but to be selected offset frequency to avoid overlapping with adjacent target echoes in the Doppler region.

Fig. 7 shows a DDMA-MIMO observation result at the height of 5.5 km, which displays the virtual receive aperture (full-synthesized) and the real aperture (used receive echoes with from A-booth transmitters only) using the same data of Fig. 5. This comparison is also suggested that narrower beam width generated by virtual antenna helps sharper Doppler spectrum width.

Generally, when the radar beam is relatively narrow (beam width is a few degrees) for the volume target, the relationship between the radar beam width and the beam broadening is known to follow an approximation of

$$\sigma_{\frac{1}{2}B} \approx \theta_{\frac{1}{2}} v_h \tag{45}$$

where $\sigma_{\frac{1}{2}B}$ is the half spectrum width of the Doppler velocity, $\theta_{\frac{1}{2}}$ is the half-power half-width of the effective radar beam, and v_h is the total background horizontal wind [19].

As shown by [20], the observed spectrum width $\sigma_{1/2}$ is expressed by the convolution of the turbulence $\sigma_{1/2turb}$ and the beam broadening as follows:

$$\sigma^2_{\frac{1}{2}} = \sigma^2_{\frac{1}{2}turb} + \sigma^2_{\frac{1}{2}B}. \tag{46}$$

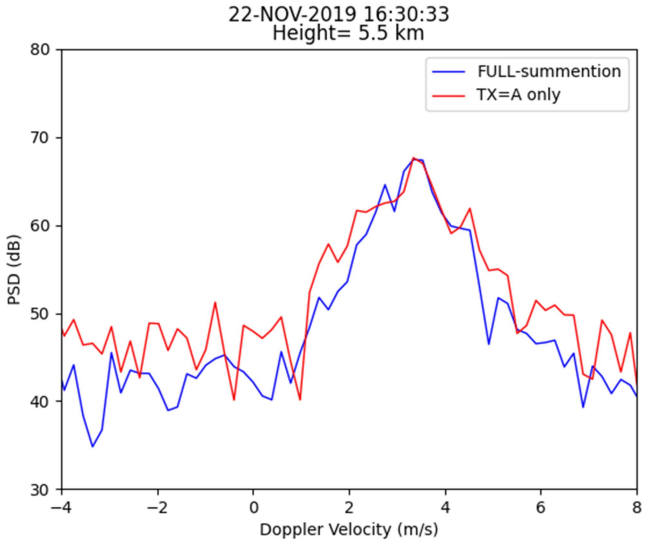

Fig. 7. Comparison between the virtual receive aperture (blue line) with the real aperture (used receive echoes with from booth A transmitters only) of the Doppler spectrum at a height of 5500 m from the ground, eastward direction of zenith angle 10° at 1630 JST November 22, 2019. Horizontal axis shows Doppler velocity, and vertical axis shows the echo power.

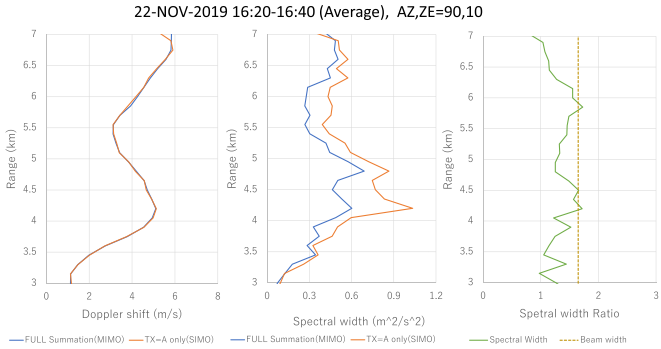

Fig. 8. Height profiles of Doppler shift (left), square of the half spectrum width (center) toward the eastward direction of zenith angle 10° observed at 1620–1640 JST November 22, 2019. The blue and the red lines show the case of full-summation (MIMO virtual) and the received data from the transmit booth A (SIMO = real aperture) with the same observation data. The right figure displays the ratio of these spectrum width, and the dotted line is the ratio of square of the array factors between these apertures, as reference.

If we regard that $\sigma_{1/2B}$ is dominant compared to $\sigma_{1/2turb}$ because of large horizontal velocities, $\sigma_{1/2B}$ is proportional to $\theta_{1/2}$, and Fig. 7 implies that this assumption is substantiated.

Fig. 8 displays height profiles of Doppler shift, square of the half spectrum width toward the eastward direction of zenith angle 10° observed at 1620–1640 JST November 22, 2019 as MIMO observation. Compared with the Doppler shift between the MIMO virtual array and real aperture (SIMO observation), these profiles are consistent. This fact indicates the Doppler shift estimation process works correctly. On the other hand, square of the half spectrum width calculated with the same process has different profiles.

As [20], observed spectrum width is greatly influenced with the antenna beam width, therefore the comparison between the

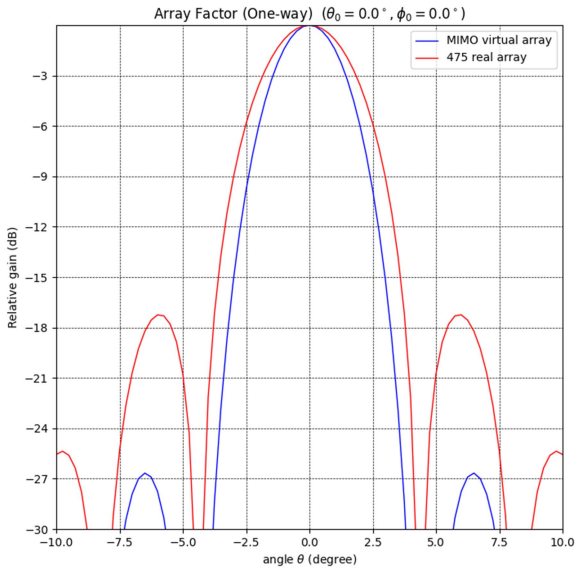

Fig. 9. Array factor. The blue and the red lines show those of the MIMO virtual and the actual antennas (SIMO), respectively.

observed spectrum width and the beam width could be a criterion. Fig. 9 displays the array factor of the MU radar. The beam width is approximately $\theta_{1/2SIMO} \approx 1.8°$ and $\theta_{1/2MIMO} \approx 1.4°$, respectively, and the ratio $\theta^2_{1/2SIMO}/\theta^2_{1/2MIMO} \approx 1.65$.

The height profile of squared spectrum width observed with the MIMO virtual and the real aperture is also shown on the right side of Fig. 8, in which the ratio of the beam width is displayed. From this figure, it can be seen that these ratios are comparable. Differences between these height profiles are estimated that turbulence component is dominant or weaker horizontal wind is affected.

As discussed earlier, these results indicate that the MIMO observation can generate narrower beam patterns. Further, we need to investigate it more quantitatively in another way.

Moreover, it may be unfair to compare MIMO and the full-array SIMO method with the identical radar as described by [8], because the MIMO radar compensates the transmit aperture and the transmit power resources with the virtual receiver aperture, which causes weak target detection ability than the identical full-array antenna system. In other words, narrower receive beam width with a virtual antenna and freedom of $M \times N$ receivers for clutter suppression are obtained in exchange for the maximum target detection range to build identical resources for the system design.

V. Conclusion

In this article, the basic principles of the MIMO radar were described, especially the DDMA-MIMO method, which utilizes pulse-to-pulse phase difference between the transmitters to achieve orthogonality. Furthermore, it was proved that a transmitter's frequency offsets could be also adopted to realize DDMA-MIMO radar.

Next, to apply the DDMA-MIMO method using the MU radar, the received MIMO signal model was expanded to L pulse trains,

and it was explained how the orthogonality characteristics were obtained using Doppler filters. In addition, the compensation method for the amplitude and phase difference of each transmitter was introduced along with the configuration of the MU radar.

Finally, the observations with the MIMO-MU radar were compared with that of the SIMO-MU radar with measuring a beam broadening effect, and the results showed that a narrower beam width is achieved using the MIMO method, which helps in creating a virtual antenna aperture plane beyond the actual antenna.

ACKNOWLEDGMENT

The MU radar belongs to and is operated by the Research Institute for Sustainable Humanosphere (RISH), Kyoto University. The authors would like to thank four anonymous reviewers whose comments helped improve and clarify this manuscript.

REFERENCES

[1] S. Fukao, T. Sato, T. Tsuda, S. Kato, K. Wakasugi, and T. Makihira, "The MU radar with an active phased array system: 1. Antenna and power amplifiers," *Radio Sci.*, vol. 20, no. 6, pp. 1155–1168, Nov. 1985.

[2] S. Kato, T. Tsuda, M. Yamamoto, T. Sato, and S. Fukao, "First results obtained with a middle and upper atmosphere (MU) radar," *J. Atmos. Terr. Phys.*, vol. 48, no. 11/12, pp. 1259–1267, 1986.

[3] H. Sun, F. Brigui, and M. Lesturgie, "Analysis and comparison of MIMO radar waveforms," in *Proc. Int. Radar Conf. Radar*, 2014, pp. 1–6.

[4] T. Y. Yu, J. I. Furumoto, and M. Yamamoto, "Clutter suppression for high-resolution atmospheric observations using multiple receivers and multiple frequencies," *Radio Sci.*, vol. 45, no. 4, pp. 1–15, 2010.

[5] J. M. Urco, J. L. Chau, M. A. Milla, J. P. Vierinen, and T. Weber, "Coherent MIMO to improve aperture synthesis radar imaging of field-aligned irregularities: First results at Jicamarca," *IEEE Trans. Geosci. Remote Sens.*, vol. 56, no. 5, pp. 2980–2990, May 2018.

[6] J. M. Urco, J. L. Chau, T. Weber, and R. Latteck, "Enhancing the spatiotemporal features of polar mesosphere summer echoes using coherent MIMO and radar imaging at MAARSY," *Atmos. Meas. Tech.*, vol. 12, no. 2, pp. 955–969, 2019.

[7] F. Li, F. He, Z. Dong, M. Wu, and Y. Zhang, "General signal model for multiple-input–multiple-output GMTI radar," *Sensors*, vol. 18, no. 8, pp. 1–20, 2018.

[8] Y. Qu, G. S. Liao, S. Q. Zhu, X. Y. Liu, and H. Jiang, "Performance analysis of beamforming for MIMO radar," *Prog. Electromagn. Res.*, vol. 84, pp. 123–134, 2008.

[9] M. S. Davis, *Principles of Modern Radar: Advanced Techniques*, M. L. William and S. A. James, Eds. Rijeka, Croatia: Scitech, 2013.

[10] M. S. Davis, G. A. Showman, and A. D. Lanterman, "Coherent MIMO radar: The phased array and orthogonal waveforms," *IEEE Aerosp. Electron. Syst. Mag.*, vol. 29, no. 8, pp. 76–91, Aug. 2014.

[11] H. D. Macedo and J. N. Oliveira, "Typing linear algebra: A biproduct-oriented approach," *Sci. Comput. Prog.*, vol. 78, no. 11, pp. 2160–2191, 2013.

[12] C. Y. Chen and P. P. Vaidyanathan, "MIMO radar ambiguity properties and optimization using frequency-hopping waveforms," *IEEE Trans. Signal Process.*, vol. 56, no. 12, pp. 5926–5936, Dec. 2008.

[13] J. Li and P. Stoica, *MIMO Radar Signal Processing*. Hoboken, NJ, USA: Wiley, 2008.

[14] V. F. Mecca and J. L. Krolik, "Slow-time MIMO STAP with improved power efficiency," in *Proc. Conf. Rec. Asilomar Conf. Signals, Syst. Comput.*, 2007, pp. 202–206.

[15] D. J. Rabideau, "Doppler-offset waveforms for MIMO radar," in *Proc. IEEE RadarCon*, 2011, pp. 965–970.

[16] M. Cattenoz, "MIMO radar processing methods for anticipating and compensating real world imperfections," Ph.D. dissertation, Université-Paris Sud-Paris XI, Orsay, France, 2015. [Online]. Available: https://tel.archives-ouvertes.fr/tel-01197253/document

[17] W. Van Rossum and L. Anitori, "Doppler ambiguity resolution using random slow-time code division multiple access MIMO radar with sparse signal processing," in *Proc. IEEE Radar Conf.*, 2018, pp. 441–446.

[18] G. Hassenpflug, M. Yamamoto, H. Luce, and S. Fukao, "Description and demonstration of the new Middle and Upper atmosphere radar imaging system: 1-D, 2-D, and 3-D imaging of troposphere and stratosphere," *Radio Sci.*, vol. 43, no. 2, pp. 1–24, Apr. 2008.

[19] W. K. Hocking, "Measurement of turbulent energy dissipation rates in the middle atmosphere by radar techniques: A review," *Radio Sci.*, vol. 20, no. 6, pp. 1403–1422, 1985.

[20] S. Fukao and K. Hamazu, *Radar for Meteorological and Atmospheric Observations*. Berlin, Germany: Springer, 2014.

Tomoya Matsuda received the B.S. degree in 1997 from the Undergraduate School of Electrical and Electronic Engineering, the Faculty of Engineering, and M.S. degree in 1999 from the Department of Electronic and Communication Engineering, the Graduate School of Engineering Kyoto University, Kyoto, Japan, where he is currently working toward the Ph.D. degree with Department of Communications and Computer Engineering, the Graduate School of Informatics.

In 1999, he joined Mitsubishi Electric Corporation, Tokyo, Japan, where he has been engaged in the development of active phased array radar system. His research interests include the development of phased array radar systems for atmospheric and weather radars.

Dr. Matsuda was the recipient of the 2022 Gambo-Tatehira Award of the Meteorological Society of Japan on behalf of Mitsubishi Electric Corporation.

Hiroyuki Hashiguchi received the bachelor of engineering degree from the Department of Electrical Engineering, the Faculty of Engineering and Design, Kyoto Institute of Technology, Kyoto, Japan, in 1990, and the Ph.D. degree from the Department of Electrical Science and Engineering, Graduate School of Engineering, Kyoto University, Kyoto, Japan, in 1995.

In 1997, he became a Research Associate with the Radio Atmospheric Science Center, Kyoto University (reorganized in 2000 as the Radio Science Center for Space and Atmosphere). In 2001, he became an Associate Professor with the Radio Science Center for Space and Atmosphere, Kyoto University [reorganized in 2004 as the Research Institute for Sustainable Humanosphere (RISH)]. In 2018, he became a Professor with RISH. His research interests include the development of atmospheric radars and research on observations using their radars.

Dr. Hashiguchi is a Member of the Meteorological Society of Japan, the Society of Geomagnetism and Earth, Planetary and Space Sciences, the American Meteorological Society, the American Geophysical Union, and the Institute of Electronics, Information and Communication Engineers, Japan. In 1992, he became the Research Fellow of the Japan Society for the Promotion of Science. He was a recipient of the 2006 Minister of Education Science and Technology Award, and the 2008 Horiuchi Award and 2022 Gambo-Tatehira Award of the Meteorological Society of Japan.